

The diffuse X-ray background

A. M. Soltan*

Nicolaus Copernicus Astronomical Center, Bartycka 18, 00-716 Warsaw, Poland

Received 13 May 2003 / Accepted 16 June 2003

Abstract. The deepest observations of the X-ray background approach the surface brightness of the truly diffuse component generated by Thomson scattering of cosmic X-ray photons. Available estimates of the electron density and the X-ray luminosity density of AGNs as a function of cosmological epoch are used to calculate the integral scattered X-ray background component. It is shown that the scattered component constitutes 1.0–1.7% of the total background, depending on the AGN cosmic evolution. Albeit this is a minute fragment of the total flux, it becomes a perceptible fraction of the still unresolved part of the background and should be taken into account in the future rigorous assessments of the X-ray background structure. This diffuse component at energies ≤ 1 keV sums up with the emission by WHIM to 3–4%. Consequently, one should expect that integrated counts of discrete sources account for just 96–97% for soft background and $\sim 99\%$ at higher energies.

Key words. X-rays: diffuse background

1. Introduction

Most of the X-ray background (XRB) is generated by discrete extragalactic sources (e.g. Campana et al. 2001; Rosati et al. 2002, and references therein). Among those sources, various classes of AGNs constitute a dominating part. Probably 5 to 10% of the soft XRB is produced by hot gas in clusters of galaxies. Hydrodynamical simulations of the evolution of the primordial gas demonstrate that some contribution to the XRB is generated by the baryonic matter which fills intergalactic space in the form of moderately hot plasma (Cen & Ostriker 1999; Davé et al. 2000; Bryan & Voit 2001; Croft et al. 2001). Due to its low density, thermal emission of this gas is extremely weak and the very existence of the “warm” baryons still waits for definite observational confirmation (e.g. Soltan et al. 2002). Thus, apart from this small constituent, it is generally accepted that the XRB is produced by discrete sources. This notion has been strengthened directly by deep observations by *ROSAT* and more recently by *Chandra*.

A relationship between the total XRB flux and integrated flux produced by sources has been investigated in detail from the observational point by Moretti et al. (2003). These authors compared the source counts with the measured XRB level in two energy bands: soft (0.5–2 keV) and hard (2–10 keV). They have shown that in the soft band the source counts integrated down to the *Chandra* limit of 2.4×10^{-17} erg s $^{-1}$ cm $^{-2}$ produce $94.3^{+7.0}_{-6.7}\%$ of the XRB. A smooth extrapolation of counts down to $\sim 3 \times 10^{-17}$ erg s $^{-1}$ cm $^{-2}$ generates 96% of the XRB and is “consistent with its full value at 1 σ level”. In the hard band discrete sources generate at most 93% (after source counts extrapolation) and are “only marginally consistent” with the

XRB level. One should note also that the total XRB flux itself is not well determined; according to Moretti et al. (2003) the uncertainties of the XRB in both bands amount roughly to 5%.

Although the present data do not allow definite conclusions, it is possible that the apparent deficiency of the source counts contribution to the hard band could be removed by steepening of counts below the present threshold of 2.6×10^{-16} erg s $^{-1}$ cm $^{-2}$. Such steepening is in fact predicted by recent evolutionary models of the obscured AGNs (e.g. Franceschini et al. 2002).

Since the deepest observations allow only for a few percent of the XRB in the form of genuine diffuse radiation, it is worthwhile to examine also those emission mechanisms which generate a weak signal as compared to the total XRB flux, but which potentially could contribute significantly to the diffuse component. The aim of the present paper is to estimate the flux of the truly diffuse emission produced by Thomson scattering of X-rays in intergalactic space. The amplitude of the integrated scattered flux depends on the cosmic history of the XRB and on the density of free electrons as a function of redshift. These functions are investigated in Sects. 2 and 3, respectively. In Sect. 4 the amplitude of the scattered component is calculated and it is discussed what constraints on the faint end of the source counts are imposed by the present results.

Most of the AGN-related XRB is generated at redshifts smaller than ~ 3 with practically no contribution at redshifts greater than 6. Since cumulative Thomson scattering optical depths at redshift 3 and 6 do not exceed respectively ~ 0.02 and 0.03 (Cen 2003), the effects of X-ray absorption remain low and the calculations below do not include effects of multiple scattering of X-rays. Integration of the radiative transfer is reduced to calculations of the XRB intensity as a function

* e-mail: soltan@camk.edu.pl

of redshift and then integration over redshift of the scattered component.

2. AGN luminosity density and the X-ray background

2.1. Local XRB

The relationship between the average X-ray background intensity and redshift is investigated. The XRB flux in the local universe is known with relatively high accuracy (e.g. Moretti et al. 2003, and reference therein). It is established that a large fraction of the local XRB is produced by AGNs distributed over a wide range of redshifts. Due to the strong cosmic evolution of the AGN population, the XRB varied substantially in the past cosmological epochs and AGNs constituted a dominating source of the X-ray radiation for most of the lifetime of the universe. In the present estimates only the AGN contribution to the XRB is considered, although some other classes of objects such as young galaxies could contribute to the XRB at high redshifts.

Observed locally at energy E the XRB flux $I_0(E)$ is equal to the integrated flux produced by sources along the line of sight:

$$I_0(E) = \int_0^{z_{\max}} dz \frac{dV}{dz} \frac{\mathcal{L}_z(E') \cdot (1+z)}{4\pi D_L^2}, \quad (1)$$

where V is the co-moving volume, D_L is the luminosity distance, and $\mathcal{L}_z(E')$ is the luminosity density generated by AGNs at redshift z and energy $E' = E \cdot (1+z)$. The maximum redshift, z_{\max} , is the redshift at which the first AGNs began to shine. Systematic variations of the luminosity density with redshift are described by the cosmic evolution $\mathcal{E}(z)$:

$$\mathcal{L}_z = \mathcal{L}_0 \cdot \mathcal{E}(z). \quad (2)$$

Various models for $\mathcal{E}(z)$ have been proposed in the literature. The models differ between each other in details, but the general shape of the evolution is common. It is accepted that at low redshifts the luminosity density generated by AGNs rises sharply, stabilizes at moderate redshifts and probably decreases at high redshifts. One should note that in the present investigation the integrated luminosity density as a function of redshift is the only ‘‘interesting’’ quantity. Thus, neither the exact shape of the X-ray luminosity function nor the evolution type (*luminosity* vs. *density* evolution) affect the calculations. It was found that the Miyaji et al. (2000) estimates of the AGN luminosity function and cosmological evolution can be used to determine the luminosity density in a straightforward and effective way. Their *Luminosity Dependent Density Evolution* model (designated as LDDE1) is applied. It is based on the combined shallow and deep *ROSAT* surveys and adequately reproduces both the source counts and the AGN redshift distribution.

The present calculations cover a wide range of redshifts. The observed energy band $[E_1, E_2]$ corresponds to the band $[E_1(1+z), E_2(1+z)]$ at the source. Since the observed flux results from the integrated emission along the line of sight, the relevant luminosity function and evolution are defined in the (redshifted) source frame (see discussion in Miyaji et al. 2000). In the paper the soft X-ray band 0.5–2 keV is used as reference

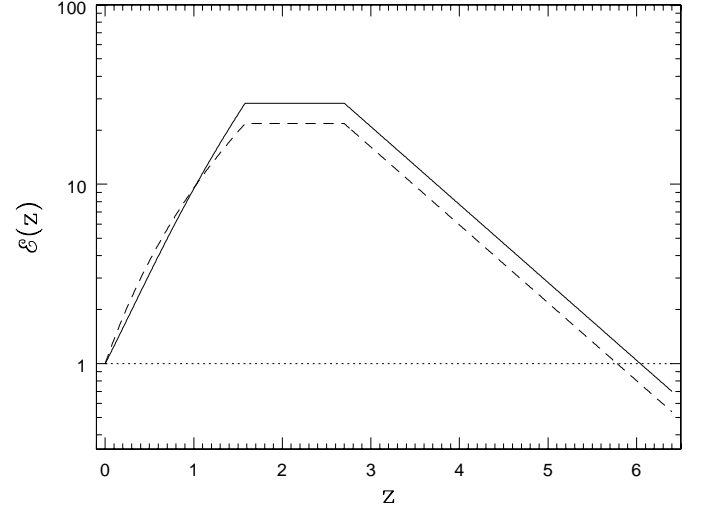


Fig. 1. Rate of the cosmological evolution of the luminosity density according to the LDDE1 model with a decline given in Eq. (3) by Miyaji et al. (2000) (solid) and density evolution by Boyle et al. (1994) (dashed).

and all the data extracted from the literature are corrected to this standard band.

The AGN sample used in the Miyaji et al. (2000) analysis contained a limited number of high redshift QSOs (17 with $z > 2.2$). In effect, constraints on the evolution rate at high redshifts are not restrictive. Miyaji et al. (2000) note, however, that the X-ray data are consistent with the decline of the space density of optically selected QSO for redshifts greater than ≈ 2.7 . To account for this trend, the evolution function, $\mathcal{E}(z)$, is calculated from the LDDE1 model with an additional ‘‘damping factor’’:

$$\mathcal{E}_z \sim \exp(2.7 - z) \text{ for } z > 2.7. \quad (3)$$

The cosmological model $(\Omega_m, \Omega_\Lambda) = (0.3, 0.7)$ has been used in all the calculations. In Fig. 1 the evolution rate defined as a ratio of the co-moving luminosity density at redshift z to its local value is shown for the LDDE1 model. The density evolution derived by Boyle et al. (1994) is plotted for comparison. Differences between both evolution laws of $\sim 25\%$ which arise at $z \gtrsim 1.5$ indicate the level of uncertainties involved in the evolution estimates (see below).

A relationship between volume, distance and redshift for the cosmological model used in the paper is taken from Hogg (1999):

$$\frac{dV}{dz} \frac{1}{D_L^2} = \omega \frac{c}{H_0} \frac{1}{F_0(z)(1+z)^2}, \quad (4)$$

where

$$F_0(z) = \sqrt{\Omega_m(1+z)^3 + \Omega_\Lambda} \quad (5)$$

with $\Omega_m = 0.3$ and $\Omega_\Lambda = 0.7$. Equations (4) and (5) inserted into Eq. (1) give for unit solid angle $\omega = 1$ sr:

$$I_0(E) = \frac{1}{4\pi} \frac{c}{H_0} \mathcal{L}_0(E) \int_0^{z_{\max}} dz \frac{\mathcal{E}(z)}{F_0(z)(1+z)^2}. \quad (6)$$

The local background flux $I_0(E)$ is only weakly dependent on the maximum redshift in the integral and in all the calculations $z_{\max} = 6$ was put. The local luminosity density and evolution have been computed from the Miyaji et al. (2000) formulae and inserted into Eq. (6). The results are dependent on extrapolation of the X-ray luminosity function (XLF) at the low luminosity end. In the present calculations the XLF is integrated over the luminosity range actually covered by the Miyaji et al. (2000) sample, i.e. between $L_{\min} = 10^{41.5} h_{50}^{-2} \text{ erg s}^{-1}$ and $L_{\max} = 10^{47} h_{50}^{-2} \text{ erg s}^{-1}$, where $h_{50} = H_0/50 \text{ km s}^{-1} \text{ Mpc}^{-1}$. In the energy band of 0.5–2 keV the AGNs according to the LDDE1 with the decline described by Eq. (3) model produce a background flux of $1.97 \times 10^{-8} \text{ erg s}^{-1} \text{ cm}^{-2} \text{ sr}^{-1}$. Using the Moretti et al. (2003) estimate of the total soft XRB at $2.47 \times 10^{-8} \text{ erg s}^{-1} \text{ cm}^{-2} \text{ sr}^{-1}$, it gives the AGN contribution at $\sim 80\%$. A pure LDDE1 model (without decline of luminosity density at high redshifts) generates a flux of $2.16 \times 10^{-8} \text{ erg s}^{-1} \text{ cm}^{-2} \text{ sr}^{-1}$ (=88% of the total XRB).

2.2. XRB in the past

A hypothetical observer at redshift z would detect the integrated XRB appropriate for his epoch:

$$I'_z(E') = \int_0^{z_{\max}} dz' \frac{dV'}{dz'} \frac{\mathcal{L}'_{z_1}[E'(1+z')](1+z')}{4\pi D_L'^2}, \quad (7)$$

where primes (') indicate that all quantities refer to and are measured by the observer at redshift z . Photons emitted at redshift z' were sent at an epoch, which for us corresponds to the redshift z_1 :

$$1 + z_1 = (1 + z) \cdot (1 + z'). \quad (8)$$

The cosmological parameters in Eq. (7) satisfy relationships analogous to Eqs. (4) and (5):

$$\frac{dV'}{dz'} \frac{1}{D_L'^2} = \omega \frac{c}{H_z} \frac{1}{F_z(z')(1+z')^2}, \quad (9)$$

and

$$F_z(z') = \sqrt{\Omega'_m(1+z')^3 + \Omega'_\Lambda}. \quad (10)$$

Standard relationships (e.g. Hogg 1999) give:

$$H_z = H_0 \cdot F_0(z), \quad (11)$$

$$F_0(z_1) = F_0(z) \cdot F_z(z'), \quad (12)$$

$$\mathcal{L}'_{z_1} = (1+z)^3 \mathcal{L}_{z_1}, \quad (13)$$

$$I'_z(E') = \frac{1}{(1+z)^2} I_z(E'), \quad (14)$$

where $I'_z(E')$ is the XRB flux per proper unit surface measured by observer at redshift z and $I_z(E')$ represents flux per co-moving unit surface. Using Eqs. (8)–(14) we finally get:

$$J_z(E'_1, E'_2) = \frac{c}{H_0} (1+z) \mathcal{L}_0(E_1, E_2) \int_0^{z_{\max}} dz' \frac{\mathcal{E}_0(z_1)}{F_0(z_1)(1+z')^2}, \quad (15)$$

where $J_z(E'_1, E'_2)$ is the XRB flux per co-moving unit surface measured at redshift z within the energy band E'_1 – E'_2 multiplied by a solid angle of 4π .

3. Electron density in intergalactic space

Extensive hydrodynamical simulations of the matter distribution (e.g. Valageas et al. 2002 and references therein) show that a dominating fraction of all the baryonic matter in the universe resides outside galaxies and cluster of galaxies. In the local universe baryons accumulated in these objects constitute $\sim 30\%$ of the total baryonic mass, while the remaining $\sim 70\%$ still stays in the *diffuse* and *warm-hot* phases filling 99% of volume space. The fraction of the diffuse components rises with redshift and reaches roughly 99% at $z = 3$ (Cen & Ostriker 1999; Davé et al. 2000). Intergalactic matter is virtually fully ionized up to $z \approx 6$ (e.g. Cen 2003).

Estimates of the total baryonic mass based on *WMAP* observations give $\Omega_b = 0.044$ for $H_0 = 71 \text{ km s}^{-1} \text{ Mpc}^{-1}$ (Spergel et al. 2003). Using results on the fraction of baryons in the intergalactic space by Cen & Ostriker (1999), the *WMAP* data give the local average electron density at $n_e(0) = 2.2 \times 10^{-7} \text{ cm}^{-3}$. Due to systematic increase of the diffuse component with redshift, the electron co-moving density rises to $n_e(z) = 2.2 \times 10^{-6} \text{ cm}^{-3}$ at $z = 1$ and to $n_e(z) = 2.0 \times 10^{-5} \text{ cm}^{-3}$ at $z = 3$. At still higher redshifts, practically all baryons reside in the diffuse component and $n_e(z) \sim (1+z)^3$.

4. The scattered component

The luminosity density generated by the Thomson scattering of the XRB is given by:

$$\mathcal{L}_z^T = n_e(z) \sigma_T J_z, \quad (16)$$

where $\sigma_T = 6.65 \times 10^{-25} \text{ cm}^2$ is the Thomson cross-section. The XRB flux due to Thomson scattering is calculated using an equation analogous to Eq. (6):

$$I_0^T(E_1, E_2) = \frac{1}{4\pi} \frac{c}{H_0} \int_0^{z_{\max}} dz \frac{\mathcal{L}_z^T(E'_1, E'_2)}{F_0(z)(1+z)^2}. \quad (17)$$

Due to the strong dependence of the electron density on redshift, the scattered component is generated primarily at high redshifts. The standard LDDE1 model with constant luminosity density for $1.6 < z < 6$ represented by the dotted curve in Fig. 2 generates scattered XRB flux of $4.14 \times 10^{-10} \text{ erg s}^{-1} \text{ cm}^{-2} \text{ sr}^{-1}$, which accounts for 1.7% of the total XRB. If the AGN luminosity density declines exponentially for redshifts $z > 2.7$ according to Eq. (3) (solid curve in Fig. 2), the scattered XRB flux is reduced to $2.42 \times 10^{-10} \text{ erg s}^{-1} \text{ cm}^{-2} \text{ sr}^{-1}$ or 0.98% of the total XRB.

Low optical depth for Thomson scattering for $z < 6$ implies relatively weak signal of the scattered XRB component. However, in the deepest exposures of the present-day instruments just a few percent of the soft XRB remain unresolved into discrete sources. Thus, the scattered component contributes measurably to the unresolved part. Moreover, a separate diffuse contribution by the WHIM is expected in the soft XRB. The amplitude of this component has not been determined yet with reasonable accuracy (Soltan et al. 2002). The WHIM contribution to the XRB is expected to drop sharply with redshift (Cen & Ostriker 1999) and it is likely that thermal emission in the 0.5–2.0 keV band does not exceed 2–3%

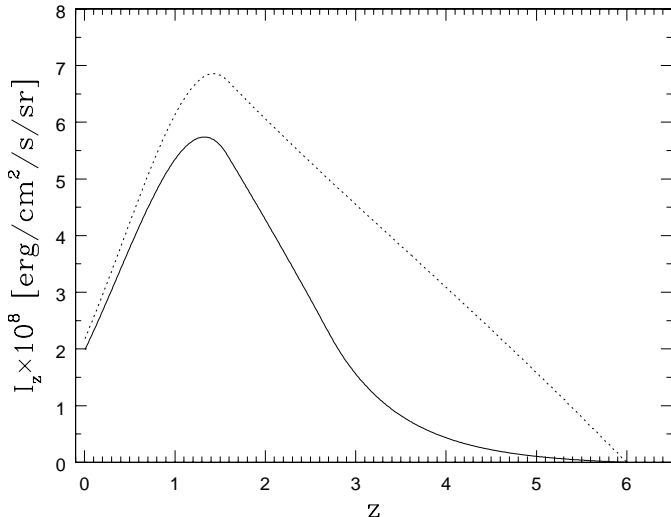


Fig. 2. XRB flux in the band $0.5(1+z)$ keV– $2.0(1+z)$ keV per comoving cm^2 measured at redshift z . The solid curve represents data for the LDDE1 model with decreasing luminosity density according to Eq. (3), the dotted curve – the LDDE1 model without “damping”. In both cases the luminosity density is set to zero for $z > 6$.

of the total XRB. Moretti et al. (2003) point out that a smooth extrapolation of the counts down to a flux level of $\sim 3 \times 10^{-18} \text{ erg s}^{-1} \text{ cm}^{-2} \text{ sr}^{-1}$, i.e. a factor of 10 below the present limits could account for 96% of the total XRB. Although this estimate is subject to relatively high uncertainties ($\sim 7\%$ at the 1σ level), the existence of the diffuse component further strengthens the conclusion that with a moderate extrapolation of source counts, all constituents of the XRB are accounted for and there is no room for new classes of X-ray sources. In particular, in the soft band the source counts cannot exhibit steepening which would increase the integrated XRB more than a few percent.

In the harder band of 2–10 keV source counts extrapolated down to fluxes an order of magnitude below the present threshold generate $\sim 93\%$ of the total XRB (Moretti et al. 2003). The relative contribution of the Thomson scattered component in this band is similar to the contribution in soft X-rays, while the expected WHIM emission above 2 keV is negligible. Thus, taking into account the diffuse component does not change the Moretti et al. (2003) conclusion that the source counts are likely to steepen below $\sim 10^{-15} \text{ erg s}^{-1} \text{ cm}^{-2}$ due to a population of highly obscured, hard sources.

Taking into account the uncertainties of the absolute flux of the total XRB and uncertainties of the discrete source contribution, which both are at the level of several percent, calculations in the present paper do not address the question whether the source counts match exactly the observed XRB. One should

stress that the objective of the present investigation was to estimate the amount of the diffuse XRB component generated by Thomson scattering. The amplitude of this component is calculated using the AGN X-ray luminosity function and evolution. The uncertainty of the diffuse component flux results mainly from uncertainties related to the evolution of the AGN population. The present calculations show that the Thomson scattered flux amounts to or slightly exceeds 1% of the total XRB. Thus, as long as uncertainties of the relevant measurements are subject to larger errors, this component does not affect decisively the XRB budget. Nevertheless, in the soft band the Thomson component narrows noticeably the distance between the resolved and total XRB and reduces the range of the allowed $\log S - \log N$ relationships. One might expect that the relative importance of the Thomson component will grow with a further increase of the resolved fraction of the background.

Direct detection of the scattered component poses a serious observational problem. This is because the spectral shape of the scattered flux strictly corresponds to the average AGN spectrum and the diffuse component mimics a population of unresolved AGN-like sources. The amplitude of the diffuse flux could be determined only indirectly by subtraction of the discrete source contribution from the total XRB. In practical terms, to establish precisely the flux produced by discrete sources one needs to determine the $\log N - \log S$ relationship well below the present limits.

Acknowledgements. This work has been partially supported by the Polish KBN grants 5 P03D 022 20 and PBZ-KBN-054/P03/2001.

References

- Boyle, B. J., Shanks, T., Georgantopoulos, I., Stewart, G. C., & Griffiths, R. E. 1994, *MNRAS*, 271, 639
- Bryan, G. L., & Voit, G. M. 2001, *ApJ*, 556, 590
- Campana, S., Moretti, A., Lazzati, D., & Tagliaferri, G. 2001, *ApJ*, 560, L19
- Cen, R. 2003, *ApJ*, 591, L5
- Cen, R., & Ostriker, J. P. 1999, *ApJ*, 514, 1
- Croft, R. A. C., Di Matteo, T., Davé, R., et al. 2001, *ApJ*, 557, 67
- Davé, R., Cen, R., Ostriker, J. P., et al. 2000, *ApJ*, 552, 473
- Franceschini, A., Braitto, V., & Fadda, D. 2002, *MNRAS*, 335, L51
- Hogg, D. W. 1999 [astro-ph/9905116]
- Miyaji, T., Hasinger, G., & Schmidt, M. 2000, *A&A*, 353, 25
- Moretti, A., Campana, S., Lazzati, D., & Tagliaferri, G. 2003, *ApJ*, 588, 696
- Rosati, P., Tozzi, P., Giacconi, R., et al. 2002, *ApJ*, 566, 667
- Soltan, A. M., Freyberg, M., Hasinger, G., et al. 2002, *A&A*, 395, 475
- Spergel, D. N., Verde, L., & Peiris, H. V. 2003, *ApJ*, accepted [astro-ph/0302209]
- Valageas, P., Schaeffer, R., & Silk, J. 2002, *A&A*, 388, 741